Applied Materials Today 27 (2022) 101437

Contents lists available at ScienceDirect

Applied Materials Today

journal homepage: www.elsevier.com/locate/apmt

Magneto-mechanical system to reproduce and quantify complex strain patterns in biological materials

Miguel Angel Moreno-Mateos[a,1], Jorge Gonzalez-Rico[a,1], Emanuel Nunez-Sardinha[b], Clara Gomez-Cruz[a], Maria Luisa Lopez-Donaire[a], Sergio Lucarini[a,c], Angel Arias[a], Arrate Muñoz-Barrutia[d,e], Diego Velasco[d,e], Daniel Garcia-Gonzalez[a,*]

[a] Department of Continuum Mechanics and Structural Analysis, Universidad Carlos III De Madrid, Avda. de la Universidad 30, Leganés, Madrid 28911, Spain
[b] Bristol Robotic Laboratory, University of the West of England, Bristol BS16 1QY, UK
[c] Department of Civil and Environmental Engineering, Imperial College London, London SW7 2AZ, UK
[d] Department of Bioengineering and Aerospace Engineering, Universidad Carlos III De Madrid, Avda. de la Universidad 30, Leganés, Madrid 28911, Spain
[e] Instituto De Investigacion Sanitaria Gregorio Marañon, Madrid, Spain

ARTICLE INFO

Article history:
Received 24 December 2021
Revised 24 February 2022
Accepted 2 March 2022

Keywords:
Magneto-active materials
Multifunctional substrates
Mechanobiology
Computational modeling
Biomechanical stimulation

ABSTRACT

Biological cells and tissues are continuously subjected to mechanical stress and strain cues from their surrounding substrate. How these forces modulate cell and tissue behavior is a major question in mechanobiology. To conduct studies under controlled varying physiological strain scenarios, a new virtually-assisted experimental system is proposed allowing for non-invasive and real-time control of complex deformation modes within the substrates. This approach is based on the use of extremely soft magneto-active polymers, which mimic the stiffness of biological materials. Thus, the system enables the untethered control of biological substrates providing reversible mechanical changes and controlling heterogeneous patterns. Motivated on a deep magneto-mechanical characterization across scales, a multi-physics and multi-scale in silico framework was developed to guide the experimental stimulation setup. The versatility and viability of the system have been demonstrated through its ability to reproduce complex mechanical scenarios simulating local strain patterns in brain tissue during a head impact, and its capability to transmit physiologically relevant mechanical forces to dermal fibroblasts. The proposed framework opens the way to understanding the mechanobiological processes that occur during complex and dynamic deformation states, e.g., in traumatic brain injury, pathological skin scarring or fibrotic heart remodeling during myocardial infarction.

1. Introduction

Tremendous research efforts are dedicated to unravelling the effects of mechanics in biology such as alterations in functional responses, morphological changes and the influence on migration, growth or healing processes [1–6]. However, there are still significant limitations to evaluating biomechanical effects and applying defined mechanical stimuli for quantitative analysis. Critical limitations are related to the isolation, combination and non-invasive control of the aimed mechanical actions affecting the biological structure of interest. Current approaches are based on polymeric substrates for cell culture and the direct application of mechanical loading on them [7–11]. However, this kind of system is limited to rather simple deformation modes and rarely allows for a combination of them (neither sequentially nor simultaneously). This limitation hinders the analysis and deep understanding of mechanical scenarios where complex deformation states evolve over time. See relevant physiological scenarios in the literature [12–15]. Among these, closed-head impacts lead to heterogeneous strain distributions that rapidly evolve resulting in significant alterations in physiological behavior [16,17]. Scarring processes (e.g., cardiac, glial, or dermal) inducing stiffness gradients within the tissue also lead to heterogeneous strain patterns resulting in temporal-varying inter-

Abbreviations: MRE, Magnetorheological elastomer; MAP, Magneto-active polymer; FEM, Finite element method.

Patent: Subject matter from this paper forms part of Patent Application No. EP22382103.4 filed on 9 February 2022 in the name of Universidad Carlos III de Madrid.

* Corresponding author.
E-mail address: danigarc@ing.uc3m.es (D. Garcia-Gonzalez).

[1] These authors contributed equally to this work.

https://doi.org/10.1016/j.apmt.2022.101437

action forces between the extracellular matrix (ECM) and the cellular systems [18,19]. Moreover, other relevant biological processes such as neural crest cell migration during development are also highly influenced by tissue stiffening and complex deformation modes associated with a gradual organization and enrichment of collagen fibers [20–22]. Another limitation of most of the current mechanical-stimulation systems is that they require direct (invasive) contact with the cellular substrate, hence risking to contaminate and introduce local damage to the matter.

More sophisticated solutions include photo-activation of changes in material properties [23], but are limited by the low penetration depth of visible light in the material and surrounding medium. To overcome these issues, some authors have proposed the use of magneto-responsive substrates [24,25]. However, these approaches were limited to overall stiffness changes and the control of different deformation modes was not allowed. Uslu and coauthors have recently developed a wireless microactuator to study mechanobiology, which is based on a hydrogel substrate connected to a permanent magnet [26]. This has provided a novel *in vitro* system but whose mechanical stimulation is constrained to a specific deformation mode. Another recent use of magneto-mechanical coupling is the development of soft robots, driven by external magnetic fields, to interact with biological tissues [27,28]. However, to the best of the authors' knowledge, there is no available methodology to conduct mechanobiological studies under controlled complex and time-varying deformation scenarios.

In this work, we aim at changing the paradigm by developing a novel experimental-computational framework that allows for non-invasive and real-time control of complex deformation modes within the cellular substrates. The system allows for instantaneous evaluation of mechanical effects and for influencing different biological responses while recording the whole temporal event. The non-invasive stimulation is possible thanks to the ability of certain materials, i.e., magnetorheological elastomers (MREs), to respond mechanically to external magnetic fields [29,30]. These MREs consist of a soft polymeric matrix (i.e., PDMS) filled with micron-size magnetic particles (i.e., carbonyl iron powder). When imposing an external magnetic field, the particles magnetize leading to internal forces in the form of particle interactions. These forces are transmitted to the elastomeric matrix causing a mechanical deformation and/or changes in the rheological properties of the MRE (i.e., stiffness). Therefore, the overall response of the MRE depends on different factors: the nature of the elastomeric matrix and magnetic particles, distribution of the particles within the matrix, mechanical boundary conditions (BCs) and external magnetic fields. A special remark relates to the mechanical BCs, as these define the coupled response of the composite: (i) if fixed BCs are imposed, the sample does not deform but experiences internal stress. Thus, if the elastomeric matrix presents a nonlinear mechanical behavior, the result of the magnetic field application is a variation in apparent material stiffness; (ii) if free BCs are imposed, the internal stresses within the MRE due to the application of the magnetic field result in mechanical deformation (i.e., change in shape).

For the development of such a stimulation framework, we have designed a multi-component stimulator-imaging system. It uses the multifunctional properties of MREs to control cellular substrates' mechanical deformation (allowing for the temporal programming of complex deformation modes) in a non-invasive manner. To carry out the work, we first manufactured different MREs varying their stiffness and the intensity of their magneto-mechanical coupling. These materials were extensively characterized at both macroscopic and microscopic scales, unveiling the mechanisms that govern their behavior. Motivated on these analyses, a multi-physics *in silico* framework was developed to act as guidance for the experimental stimulation setup. This provides the controlling parameters to induce desired magnetic fields on the MRE-cellular substrate, and the subsequent mechanical deformation to be transmitted to the biological matter. The viability and versatility of the complete experimental-computational framework for *in vitro* mechanical stimulation of cellular systems were finally assessed by two applications taken as proof of concept. First, the ability of the system to reproduce complex mechanical scenarios was demonstrated by simulating a set of local strain patterns occurring within the brain tissue during a head impact. Then, the capability of the framework to transmit mechanical forces to cellular systems was evaluated by subjecting primary human dermal fibroblasts (hFBs) to magneto-mechanical loading. Differently from previous approaches in the literature, we allow at the same time for: non-invasive (through magnetic fields) mechanical stimulation, real-time control of mechanical stimulation, and alternating (complex) deformation modes controlling local changes in both magnitude and principal strain components. The proposed framework leads to novel studies to understand mechanobiological mechanisms behind relevant processes that develop under complex and dynamic deformation states (e.g., traumatic brain injury, pathological skin scarring, fibrotic heart remodeling during myocardial infarction). In addition, it opens doors for novel stimulation capabilities of biological matter.

2. Materials and methods

2.1. Magneto-mechanical biological stimulation device

We developed a multi-component stimulator-imaging system to influence *in vitro* biological responses by the application of remote magnetic fields on multifunctional substrates. The whole experimental setup is linked with an advanced computational framework that guides the controlling parameters to impose mechanical deformation patterns on the cellular substrate. Consequently, mechanical forces are transmitted to the cellular system affecting its behavior.

A magneto-stimulation device was designed to fit in an incubator allowing for the application of magnetic fields on the MRE substrate along time. The device was conceived to allow for real-time application of semi-uniform magnetic fields (reasonably uniform near the center area with magnitudes, ranging from 0 to 20 mT in vacuum and not compromising cell viability). The system is externally bounded by the incubator in the microscope (127.5 mm x 85.25 mm x 22.5 mm) and can be internally adapted to different Petri dishes up to 35 mm in diameter. Further details about the manufacturing of the device and its control algorithm can be found in Supplementary Information. To impose the magnetic conditions, our stimulation system is comprised of four independently controllable sets of permanent magnets surrounding the sample, with two sets aligned along each axis (Fig. 1). By moving the magnets closer or further from each other, we can vary the resulting field over the region of interest. The two axes lie orthogonal to control the field in each direction, with the final field obtained by superposition. The choice of permanent magnets instead of electromagnets is based on: (1) the ease of integration of the permanent magnets within the system, and (2) the reduction of heat sources due to resistive behavior of the electromagnets. As these components are within the incubator region and close to the cellular system, we opted for permanent magnets to avoid heat sources. The resultant mechanical deformation of the MRE substrate will be determined by the final field and macroscopic particle interactions due to the presence of the magnets, with the magnitude determined by their relative position to the MRE sample. Overall, local mechanical deformation of the cellular substrate can be controlled on the fly in terms of magnitude and orientation, enabling the transmision of reversible forces to cells. This device was coupled to a novel imaging setup especially built

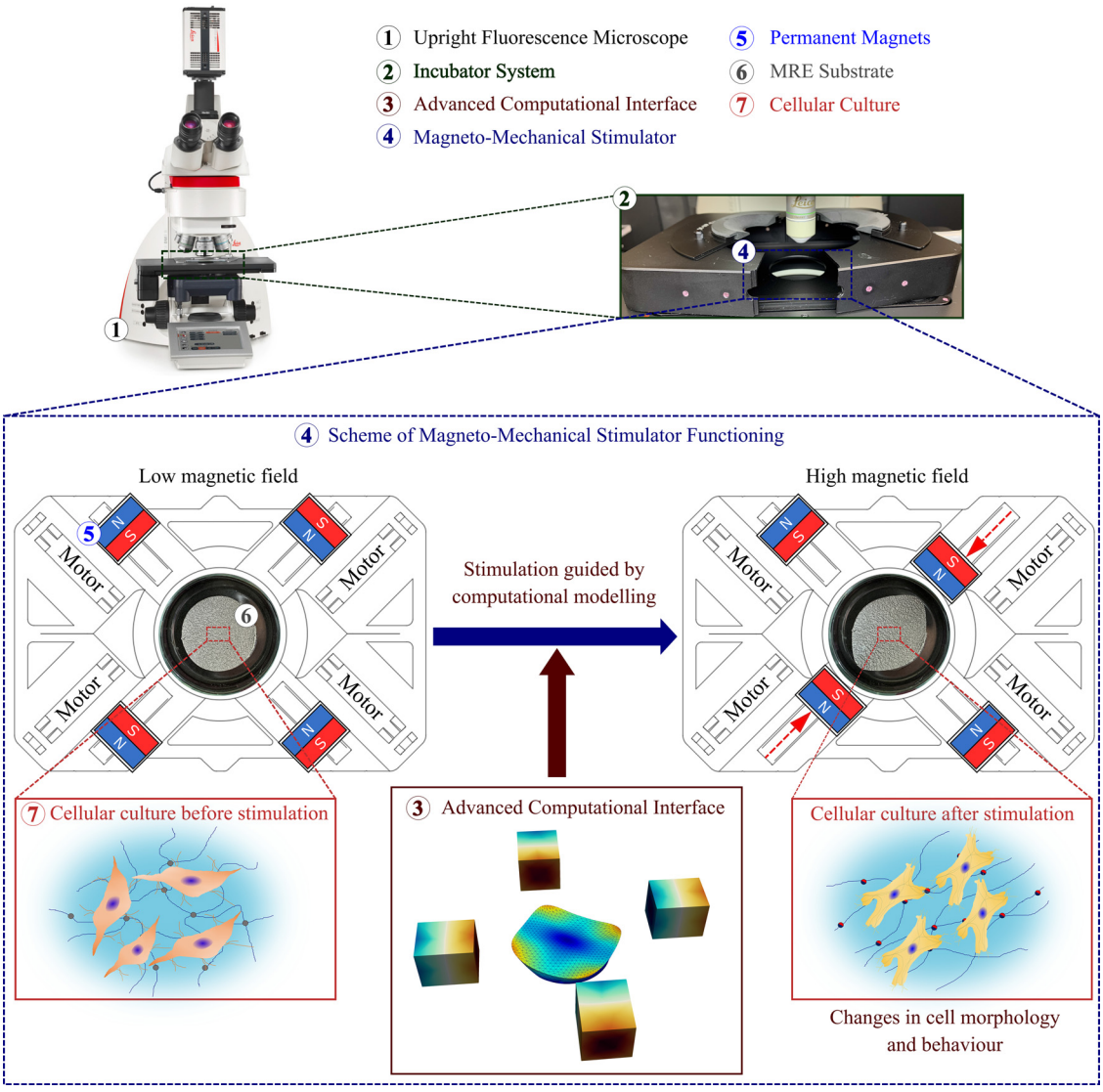

Fig. 1. Magneto-mechanical stimulation device coupled to the multidimensional imaging system. Multidimensional imaging system LEICA LAS X with an upright fluorescence microscope (with ceramic objectives) coupled to a non-ferromagnetic incubator system. The incubator system hosts a magneto-mechanical stimulation device that actuates on a magnetorheological elastomer (MRE) sample that serves as the substrate for the cellular system. The device is equipped with permanent magnets that are moved by small motors controlled by a computational-experimental interface. Based on computational simulations, the controlling system computes the permanent magnets' relative positions to generate a given magnitude and direction of the magnetic field within the MRE. The targeted magnetic field is estimated by multi-physical computational modelling to induce deformation patterns within the MRE substrate that are transmitted to the biological system cultured.

for this work (see Figs. 1 and S1). Thus, the whole framework allows for measuring cellular dynamics by means of morphological changes, proliferation or migration processes, among others.

The cellular dynamics are provided over time at both individual cell and continuum scales while controlling the magneto-mechanical interactions within the MRE substrate. While the magnetic fields can be straightforwardly tuned by the location of the permanent magnets, controlling the resulting mechanical deformation of the MRE is a challenging endeavor. Such a magneto-mechanical response is determined by numerous mechanisms that develop in parallel at both micro- and macroscales. To overcome these difficulties and provide an efficient controlling system for the substrate deformation, an advanced interface between the experimental components and computational models imposes the magneto-mechanical dynamic conditions on the MRE. In this regard, numerical simulations compute, in the presence of a given MRE sample, the effective magnetic field magnitude and direction depending on the position of the permanent magnets. Then, the subsequent deformation state within the MRE is estimated by multi-physical computational modelling taking as input the material substrate characteristics (see next sections for more details). We note that the methodology developed herein can also be used within a regular incubator, without the need for the ad-hoc microscopy system presented. Thus, the cellular system can be evaluated at different time points in any fluorescence upright microscope.

2.2. Imaging setup

The imaging setup was built with the support of Leica (Leica Microsystems, Wetzlar, Germany) and Okolab (Okolab S.R.L., Pozzuoli, Italy) companies to fulfil the following set of requirements: temporary control of temperature, CO_2 and humidity conditions during long times (> 3 days), tracking of cellular systems cultured on opaque substrates, minimization of components with medium/high magnetic permeability and non-invasive con-

trol of the magnitude and direction of magnetic fields within the cellular region. The final solution consists of a multidimensional imaging system LEICA LAS X with an upright fluorescence microscope (with ceramic, i.e., non-ferromagnetic, objectives) coupled to a non-ferromagnetic incubator (Fig. S1).

2.3. Magnetorheological elastomers preparation and functionalization

The selected MRE is composed of a soft elastomeric matrix and soft-magnetic particles. The carrier matrix, supplied in two phases, is Dowsil CY52-276 (DowSil, Midland, MI, USA) (PDMS). To reach the desired crosslinking degrees (stiffness and viscoelastic response), both phases were combined at multiple mixing ratios of 6:5, 1:1, 9:10 and 5:6, from the weakest to the strongest crosslinking, respectively. In addition, the magnetic fillers, soft SQ carbonyl iron powder (CIP) (BASF, Germany) with mean diameter 3.9–5 μm and soft-magnetization, were added to the raw mixture before the curing process. The particle's volume fractions (ϕ) of 0.15 and 0.3 were chosen to get different intensities of the magnetic interactions between the particles and mechanical stiffening. The geometry of the samples tested on the rheometer consists of cylinders with 20 mm diameter and 1 mm height. This geometry is chosen to ensure homogeneous fields during the rheological tests. For the nanoindenter, cylinders of 20 mm diameter and 4 mm height were used to replicate the testing conditions imposed in the cellular assays, and to limit the mechanical constraint due to the adhesion between the MRE sample and the base of the petri dish.

After fabrication, the MRE was sterilized with 70 % ethanol and then rinsed with water, followed by UV sterilization for 20 min. After sterilization, MREs were incubated in bovine collagen type I (Gibco (tm), FisherScientific, USA) solution diluted in PBS (0.5 mg/ml) under UV light. After 2 h, the surface of the MREs was hydrophilic, indicating a correct coating of the substrate.

2.4. Macroscopic characterization

A TA HR-20 rheometer with Magneto-Rheology Accessory from Waters TA Q600 (TA instrument, New Castle, DE, USA) was used to determine the structural response of the MRE under two deformations modes: axial compression and rotational shear. Dynamic mechanical analysis tests assessed the visco-elastic response as a function of harmonic excitation frequencies (0.01, quasi-static, to 10 Hz). At the same time, perpendicular magnetic fields of 0, 50, 100 and 200 mT were externally applied to the samples. See Supplementary Information Text for further detail.

2.5. Microscopic characterization

Micron-sized indentations were conducted with a Chiaro nanoindentation system (Optics11 Life, Netherlands) equipped with a 50 µm radius and 0.25 N/m stiffness spherical tip. Monotonous indentation measurements were performed with a final indentation depth of 10 µm and a rate of 1 µm s^{-1}. The Hertz contact model allowed to obtain the Young's modulus, E from the loading branch of the load-indentation curves. Relaxation tests started with an indentation at 20 µm s^{-1} and continued for 60 s with a constant-indentation step. Further detail about the microscopic characterization is reported in Supplementary Information Text.

2.6. Digital Image correlation analysis and postprocessing algorithms

The upper side was treated by applying a white speckle with an airbrush over the grey MRE. A CCD camera was set perpendicular to the surface so that geometric distortion of the imaging system is negligible. After acquiring the images, the NCorr open-source software package, implemented in MATLAB [31], was used to compute the displacement fields and derive the Euler-Almansi strain fields. A postprocessing algorithm corrected the translational and rotational rigid body motion of the sample during image acquisition. The resulting curves are plotted on the Frobenius norm of the strain field. See Supplementary Information Text for further detail.

2.7. Constitutive formulation of the continuum media

The magneto-mechanical problem is formulated on the deformation gradient tensor **F** and three magnetic variables, that expressed in the spatial configuration read as: the magnetic field **h**, magnetization **m**, and magnetic induction **b**. These variables can be alternatively expressed in the material configuration, respectively, as:

$$\mathbf{H} = \mathbf{h}\cdot\mathbf{F}$$

$$\mathbf{M} = \mathbf{m}\cdot\mathbf{F} \tag{4}$$

$$\mathbf{B} = \det(\mathbf{F})\mathbf{b}\cdot\mathbf{F}^{-\mathbf{T}}$$

Moreover, these variables are related in the bulk as:

$$\mathbf{B} = \det(\mathbf{F})\mu_o\mathbf{C}^{-1}(\mathbf{H}+\mathbf{M}) \tag{5}$$

where μ_o is the vacuum magnetic permeability.

The constitutive formulation for the MRE was defined within a thermodynamically consistent framework deriving the stress and magnetic components from a total energetic potential as:

$$\Psi(\mathbf{F},\mathbf{H}) = \Psi_{\text{mech}}(\mathbf{F}) + \Psi_{\text{max}}(\mathbf{F},\mathbf{H}) + \Psi_{\text{mag}}(\mathbf{F},\mathbf{H}) \tag{6}$$

where Ψ_{mech}, Ψ_{max} and Ψ_{mag} are, respectively, the mechanical (Gent model formulation), the Maxwell and the magnetization energetic contributions, that were defined as:

$$\Psi_{\text{mech}}(\mathbf{F}) = \begin{cases} -\frac{\mu J_m}{2} ln\left[1 - \frac{\text{tr}(\mathbf{F}^{\mathbf{T}}\cdot\mathbf{F})-3}{J_m}\right] & if\ det(\mathbf{F}) = 1 \\ +\infty & otherwise \end{cases}$$

$$\Psi_{\text{max}}(\mathbf{F},\mathbf{H}) = -\frac{\mu_0}{2}\mathbf{F}^{-\mathbf{T}}\cdot\mathbf{H}\cdot\mathbf{F}^{-\mathbf{T}}\cdot\mathbf{H} \tag{7}$$

$$\Psi_{\text{mag}}(\mathbf{F},\mathbf{H}) = -\mu_0\left[\frac{m_s^2}{\chi} log\left(cosh\left[\frac{\chi}{m_s}\sqrt{\mathbf{F}^{-\mathbf{T}}\mathbf{H}\cdot\mathbf{F}^{-\mathbf{T}}\mathbf{H}}\right]\right)\right]$$

where μ, m_s and χ are the shear modulus, the magnetic saturation, and the magnetic susceptibility of the MRE, respectively. The parameter J_m defines a stretching threshold associated with the extensibility limit of the material.

Therefore, similarly to the calculation of the stress tensors from thermodynamic principles in hyperelasticity, the mechanical and magnetic constitutive equations can be derived from the total energy potential as:

$$\mathbf{P} = \frac{\partial\psi(\mathbf{F},\mathbf{H})}{\partial\mathbf{F}} - p\mathbf{F}^{-\mathbf{T}}$$

$$\mathbf{B} = -\frac{\partial\psi(\mathbf{F},\mathbf{H})}{\partial\mathbf{H}} \tag{8}$$

where **P** is the first Piola-Kirchhoff stress tensor. Note that a Lagrange multiplier (p) appears in the definition of the stress to impose incompressibility condition within the MRE according to Eq. (7). It is worth mentioning that the magnetic problem allows for taking any magnetic variable as the independent one. Namely, the choice will be determined by the specific application. These constitutive equations, along with the corresponding governing equations, provide the computational framework for the

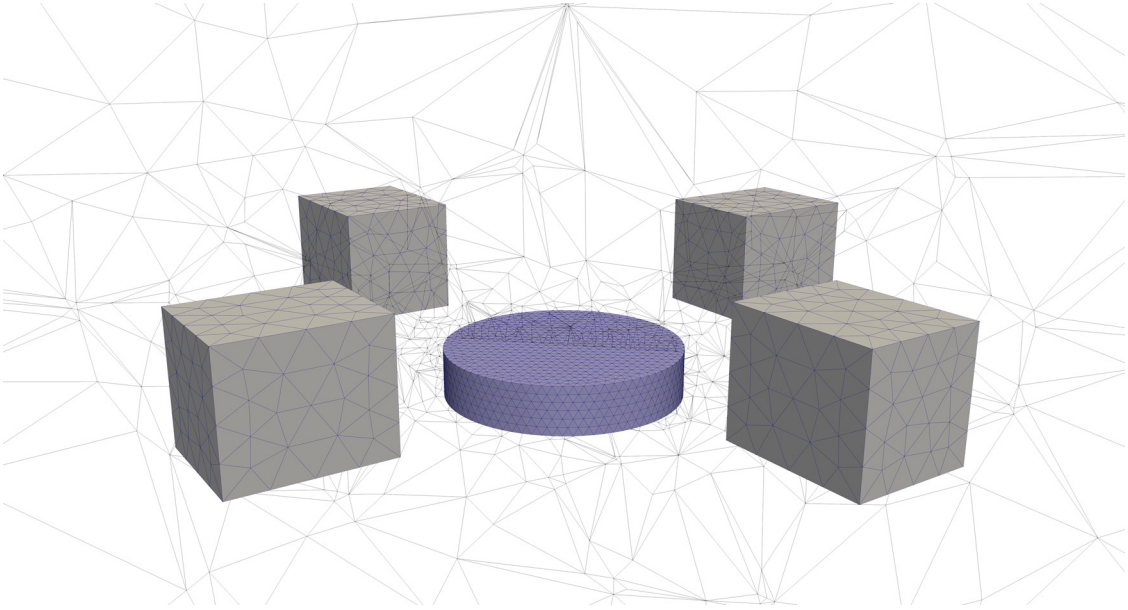

Fig. 2. Finite element mesh of the magneto-mechanical stimulation setup used in the computational simulation. A detail of the discretized domain including the MRE substrate, the four magnets and the surrounding air. The meshing of the MRE subdomain is refined to enhance the accuracy in the MRE substrate, whereas a courser meshing strategy is chosen for the magnets and further air. Note that to facilitate the visualization, the mesh of the air is presented by means of a two-dimensional clip in the middle plane.

magneto-mechanical problem. The main governing equations are the mechanical balance and magnetostatics Maxwell's equations:

$$\nabla_0 \cdot \mathbf{P} + \mathbf{f_o} = 0$$

$$\nabla_0 \cdot \mathbf{B} = 0 \tag{9}$$

$$\nabla_0 \mathrm{x} \mathbf{H} = 0$$

where ∇_0 is the material gradient and $\mathbf{f_o}$ are the external mechanical body forces.

Moreover, the magnets were mechanically defined as quasi-rigid solids, i.e., stiffness of various orders of magnitude higher than the MRE. The constitutive definition of their magnetic behavior was defined by a constant magnetization **M** equal to their residual magnetization. Then, from the magnetic field **H**, the magnetic flux density vector **B** can be computed using Eq. (5). For the description of the surrounding air, null magnetization **M** was defined along with vacuum magnetic permeability. The mechanical response of the surrounding air was defined as a compressible material with very low stiffness so that no mechanical constraints were imposed on the MRE sample [32–34].

2.8. Computational model

The simulations explicitly model the magneto-mechanical problem and replicate the experimental testing conditions of the stimulation device when actuating within the imaging system. To this end, we defined a finite element (FE) model that considers the cylindrical MRE sample, the four permanent magnets and the surrounding air. Thus, we accounted for magneto-mechanical coupling within the MRE due to magnetic field lines going through it. We also take into account macroscopic interactions between the MRE and the magnets. The domains representing the different phases are discretized in FE meshes of quadratic tetrahedral elements (Fig. 2). An adaptive meshing strategy has been used to provide finer element size in the MRE sample. After spatial convergence analysis, the full mesh comprises 32112 elements: 12171 for the MRE, 395 for each permanent magnet and 18361 for the surrounding air. For the incompressibility condition associated with the Lagrangian multiplier in Eq. (8), the discretization is reduced to the points corresponding to the tetrahedral elements' centers. The numerical implementation of the problem consists in the integration of the equilibrium equations (Eq. (9)) along with a penalty term for incompressibility. The problem was implemented in the python Finite Elements module FEniCS by symbolically indicating the weak form of those equations. The non-linear problem was solved monolithically with a Newton-Raphson procedure.

The multi-physics problem requires the definition of certain boundary conditions. In this regard, the permanent magnets were fixed (all mechanical degrees of freedom) in the target position according to the experimental condition simulated. In addition, the base of the MRE sample was mechanically fixed reproducing the experimental conditions, i.e., the MRE sample sticked to the Petri dish. To overcome convergence difficulties associated with the highly nonlinear nature of the coupled problem, the permanent magnetization of the magnets was imposed in the form of a temporal ramp until reaching the real value. Finally, the boundary of the air phase was also mechanically fixed. Note that the outer domain boundary is sufficiently remote from the volume occupied by the MRE and magnets such that the magnetic field perturbations caused by the latter practically vanish at the air boundary. As the Maxwell stress contribution is present in all domains, it was neglected in the implementation following previous works [33–35].

The permanent magnets were defined as rigid solids by constraining the displacement of all their nodes, and their residual magnetization ($\mu_0|\mathbf{M}| = 1.1$ T is defined constant) was calibrated from experiments using a Wuntronic, KOSHAVA5-USB Tesla/Gauss Meter. This calibration was validated by un-coupled magnetic FE modelling, simulating cases without MRE sample and comparing computational values of the field B with experimental measurements at different positions. The material parameters that describe the magnetic behavior of the MRE (m_s and χ) correspond to homogenized variables that account for both the elastomeric matrix and the magnetic particles. These were estimated from the homogenization approach, where only mechanical and magnetic variables

with clear physical meaning were taken. The mechanical parameters (μ and J_m) were directly taken from experimental characterization data. The model parameters used are collected in Table S1. The surrounding air is modelled as a very low stiffness material so that its contribution to the mechanical balance is negligible, but it plays a role in the magnetic problems as reported in some works [33–35]. Other alternatives to deal with higher MRE deformations would require the use of multipoint constraints or more sophisticated approaches [36–38]. To prevent excessive element distortion of the air in the regions in contact with the MRE and enhance the convergence of the model, the auxiliary energy density approach reported by Dorn et al. [39,41] was implemented. To this end, a weighting function was directly applied to the energy function on such subdomain to balance its stiffness. This modification is suitable when the air is modelled as a mesh that becomes coarser at larger distances from the magnetic body.

Further details about the full-field homogenization model can be found in Supplementary Information Text.

2.9. Cell culture

Human dermal fibroblasts were cultured before their use at 37 °C in a humidified 5 % CO2 incubator in DMEM (Gibco, Fisher Scientific, USA) supplemented with 10 % FBS (Sigma-Aldrich, USA) and 1 % Antibiotic/antimycotic (Gibco, Fisher Scientific, USA). Once ready to be cultured on the MRE, they were seeded at low density ($7{\cdot}10^3$ cells/cm^2) to allow for visualization of individual cell morphology and polarity changes rather than cell monolayer behavior. The cells seeded on top of the opaque MRE were imaged with an upright fluorescence microscope and kept in a humidified incubation chamber at 37 °C and 5 % CO_2. Details about the viability study and cell number and morphology assessment can be found in Supplementary Information Text.

2.10. Imaging analysis of cell orientation

Fibroblast alignment depending on the sensed deformation field was analyzed using the OrientationJ plug-in for Image J [40]. The orientation of the cells was characterized after 2 and 24 h of magneto-mechanical stimulations (i.e., control, static and dynamic stimulation scenarios) and compared to their original orientation before imposing the magnetic field to the MAP substrate. The orientation distribution was obtained for regions located at the center of the MAP (2) and at lateral regions subjected to high (1) and low (3) deformation fields, respectively. For each region, the distribution was calculated by normalizing and averaging distributions from three biological replicas. Polar histograms comparing the dimensionless average orientation for different stimulation conditions were computed. OrientationJ was also used to perform visual representations of cell orientation by plotting the local orientation of the cells as a hue spectrum over binary images of the segmented cells.

3. Results

3.1. Magneto-active substrates and multifunctional response

A critical component of the stimulation system is the MRE used as cellular substrate. This material mechanically responds to external magnetic stimuli and transmits the resulting forces to the cellular system cultured on its surface. To manufacture these composites, we selected an extremely soft elastomeric matrix (ultrasoft PDMS) and soft magnetic particles made of carbonyl iron powder (CIP) with a mean diameter of 5 μm (see Methods for details). The surface in contact with the cultured cellular system is treated with a collagen coating to enhance biocompatibility (see Fig. 3A). In addition, to tune the multifunctional behavior of the MREs, we characterized their magneto-mechanical response accounting for twelve different combinations of elastomeric mixing ratio (i.e., matrix stiffness) and particles' volume fraction. Note that, a priori, softer elastomeric matrices and higher particles' content lead to higher magnetorheological effects (i.e., mechanical deformation under magnetic fields and/or stiffness changes) [42]. However, we have observed non-obvious (unexpected) responses with changes in these parameters due to the complex multi-physical nature of the MRE system (see the compressive response in Fig. 3B.1).

The problem addressed in this work requires a material characterization at two different scales: macroscopic and microscopic. The magnetic problem must be solved macroscopically as it depends on the nature (i.e., permanent magnet, coil) and location of the magnetic sources as well as on the nature (i.e., material properties, geometry) and location of the MRE. The macroscopic response of the MRE is thus governed by a strong structural component, i.e., local magneto-mechanical responses are governed by the structural/macroscopic coupling in the MRE [33,42]]. To evaluate such a macrostructural response, we performed experiments in a magneto-mechanical rheometer. These experiments allowed testing the MREs under uniaxial compression and shear deformation modes in a wide range of magnetic field conditions. Moreover, the cellular system (cultured on the MRE) consists of individuals with a characteristic length in the range of microns. Therefore, the stiffness and forces/deformations transmitted to the cells are related to local (micron-size) responses. The microstructural response was evaluated by conducting nanoindentation tests at different rate conditions.

A summary with the most relevant results is provided in Fig. 3B and 3C, respectively, and the entire set of results, in Figs. S2–S7 and Tables S2–S4. In this regard, when subjected to an axial magnetic field, the MREs experienced a significant increase in stiffness that is stronger in compression than in shear loading. This effect is explained by the application of the magnetic field along the axial direction during compression loading, leading to the structural (macroscopic) response of the MRE to govern its behavior. Under shear loading, the magnetic fields play a lower role on the MRE's mechanical performance. Although a direct relationship between elastomeric mixing ratio and stiffness (under null magnetic fields) is observed in the former tests, the magneto-mechanical response under uniaxial compression loading presents complex dependencies. However, under shear loading, the effect of the mixing ratio is consistent for all the different magneto-mechanical conditions [43]. As the mechanical forces between the MRE and the biological matter will be mainly transmitted in tangential terms, these latter tests (shear) provide a more representative data set for this work [44]. Such experiments showed a magnetorheological effect (i.e., increase in stiffness) of up to 1.7 times for 50 mT and 9.3 times for 200 mT. Note that this stiffening refers to a macrostructural effect and does not imply microstructural stiffening of the elastomeric matrix. The nanoindentation tests provided a local stiffness ranging from 4.1 to 14.6 kPa depending on the mixing ratio, and a characteristic relaxation time in the order of ~0.5–1.0 s, see Table S3.

Another important fact is that the collagen coating was found to play a negligible role in material stiffness at both macro and microstructural responses. This fact indicates that the coating does not significantly affect the transmitted forces from the MRE to the biological matter. The relaxation times of MREs with higher particles' content, at the macroscopic scale, were measured reporting a significant increase up to ~10 s (see Table S2 for further detail).

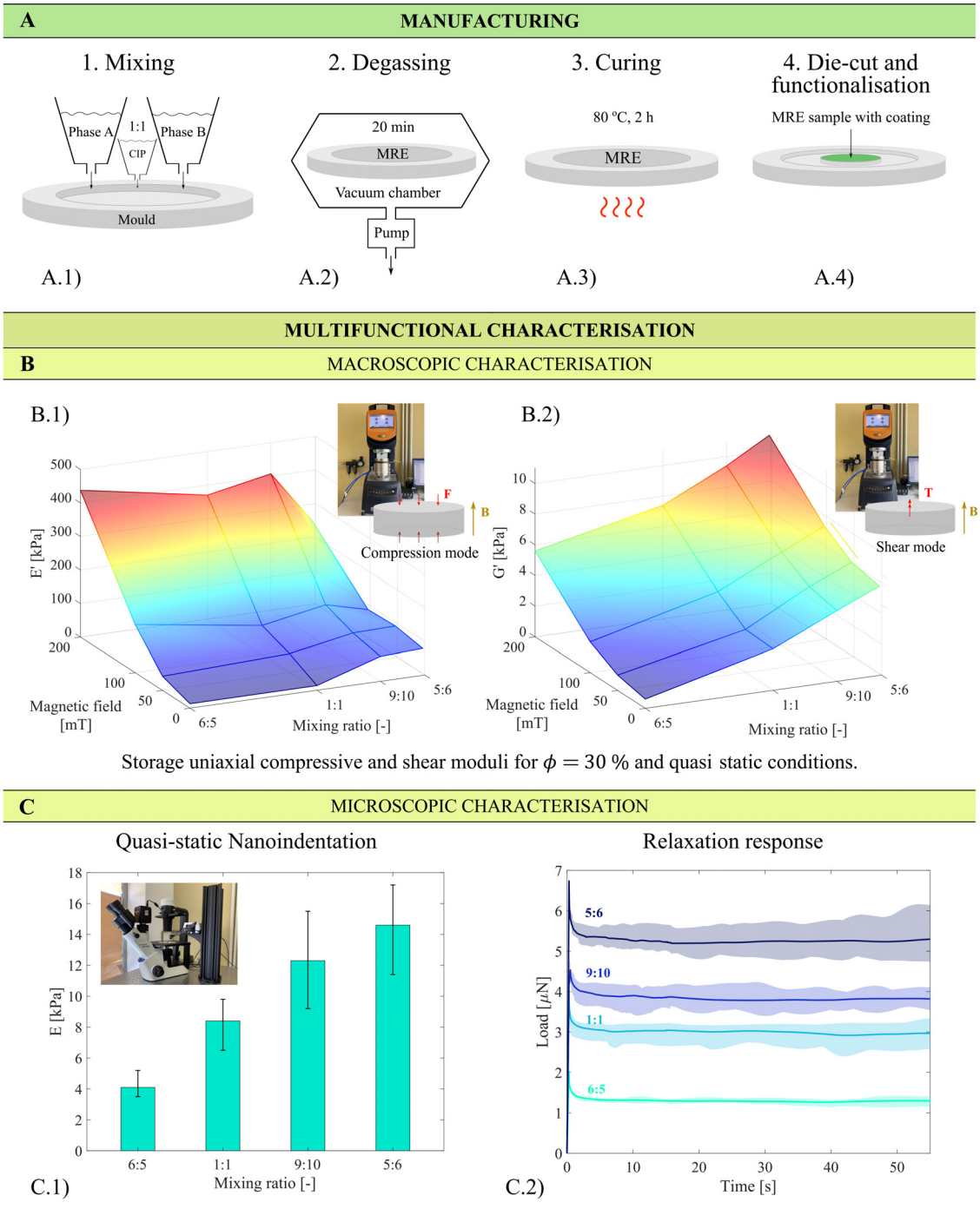

Storage uniaxial compressive and shear moduli for $\phi = 30$ % and quasi static conditions.

Nanoindentations performed on the polymeric phase. No significant changes for different particles' content and external magnetic fields (negligible strain hardening on the matrix).

Fig. 3. Manufacturing and mechanical characterization of MRE samples. (A) Scheme of the experimental manufacturing methodology divided into four stages: (A.1) mixing; (A.2) degassing; (A.3) curing; (A.4) die-cut. (B) Magneto-mechanical characterization at the macroscale by using a rheometer equipped with a magnetic device: (B.1) under uniaxial compression loading, storage Young's modulus depending on the mixing ratio used for the polymeric matric of the MRE and on the magnetic field applied; (B.2) under shear loading, storage shear modulus depending on the mixing ratio used for the polymeric matric of the MRE and on the magnetic field applied. These tests were performed under quasi-static conditions and for a magnetic particles' volume ratio of 30%. (C) Magneto-mechanical characterization at the microscale by using a nanoindentation equipment: (C.1) Young's modulus depending on the mixing ratio used for the polymeric matric of the MRE; (C.2) load versus time relaxation curves depending on the mixing ratio used for the polymeric matrix of the MRE. Note that the microscopic measurements were taken on the polymeric phase and the values measured did not show significant changes when varying the particles' content or applying external magnetic fields.

3.2. Mechanical forces within the cellular substrate due to magnetic stimulation

From the results provided in Fig. 3, we inferred a promising magnetostrictive response of the MREs (i.e., mechanical deformation under an external magnetic field), but a slight increase in microstructural stiffness (i.e., stiffening of the elastomeric phase) due to low strain-hardening (low nonlinear response). Note that, for the proposed biomechanical stimulation framework, these features must be evaluated at a microscale level (i.e., cell characteris-

tic length) [45]. To assess the micro-magnetorheological effect, we coupled the nanoindentation system to the magnetic-stimulation device presented in Fig. 1. This allows for measuring changes in stiffness due to the application of an external magnetic field. The nanoindentation results within the central region showed negligible stiffness changes due to the external magnetic fields (as expected owing to the low strain-hardening of the elastomeric matrix), Fig. 3C.

If such a device is used under free mechanical BCs, we can evaluate the mechanical deformation of the MRE due to the applied magnetic field. These experiments showed significant mechanical deformations within the MRE, see Fig. 4. Digital image correlation (DIC) was used to compute local deformation values on the top MRE surface. The plots shown in Fig. 4C, Figs. S8 and S9 present the magnitude of the local deformations according to the legend, and principal strain lines to indicate the effective force direction that the cells sense. In this regard, the magnetic-stimulation system can introduce deformation patterns in different directions of up to $>$ 30 %. It must be noted that the free-deformation tests presented significant variability when exposed to high magnetic fields with maximum relative errors of 15 %. However, these errors corresponded to the peripheral regions. Within the internal region of the MRE (up to 7.5 mm radial distance from the center), the errors were below 5 %. This behavior is explained by the strong influence of the distance to the permanent magnets on the local magneto-mechanical response of the MRE (i.e., the larger the distance, the more reproducible the deformation is).

An important feature when using the magnetic stimulation device (Fig. 1) is that the external magnetic field cannot be controlled homogenously due to fringing effects and heterogeneous magnetic permeability, hindering the analysis of the experiments. Another issue is the nonlinear coupling between magnetic fields and mechanical deformation. To help at controlling and predicting the deformation patterns transmitted to the cells during the experimental assays, we developed a 3D finite element (FE) model. The model takes the MRE material composition and geometry, as well as the position of the permanent magnets to provide: i) the spatial distribution of the magnetic fields; and ii) the resultant local deformations within the MRE. It consists of a FE model that explicitly accounts for the permanent magnets, MRE sample and surrounding air, and it couples nonlinear magnetics with nonlinear mechanics. The complete constitutive formulation and details of the integration algorithm are provided in Methods section, while a validation against experimental data by means of displacement fields at the upper MRE surface is provided in Figs. 4B and S10. This computational tool is essential to design experiments on biological systems.

Considering the (microstructural and macrostructural) experimental and computational data altogether, we found that the deformations develop as stretching along the main field direction (see an illustration of the primary mechanism governing such a response in Fig. 4A). When the permanent magnets approach the MRE, the magnetic particles start to magnetize leading to three main magneto-mechanical couplings: (i) dipole-dipole interaction between particles that result in attraction forces [46]; (ii) paramagnetic torques that lead to the formation of chain-like particles distributions and their reorientation along the external magnetic field [47]; and (iii) a strong attraction force between the particles and the magnet itself. The extremely soft nature of the elastomeric matrix facilitates the rearrangement of particles favoring the latter mechanisms and, therefore, the resulting expansion of the MRE towards the permanent magnet's location. Overall, the experimental-computational results from this section and the previous one, provide the stiffness and deformation ranges that can be reached with the magnetic stimulation system as a function of the manufacturing conditions of the MRE substrate (see Table 1).

3.3. Reproduction of complex strain fields: application of the stimulation system to reproduce complex brain strain distributions from experimental data

Resorting to a direct application of mechanical loads on a substrate, some authors have reported pure and simple mechanical stimulation frameworks [[8],10,11]. Intricate physiological strain patterns, such as myocardial tissue contractions, skin Langer lines and deformations on the brain due to closed head impact, however, require novel experimental frameworks. They need not only to reproduce these patterns, but also to control and adapt them over time [48]. Here, we demonstrate the versatility of our system to, fed by *in vivo* experimental strain distributions, reproduce a real mechanical event along time.

We have proved our system to be able to reproduce brain strain patterns during closed head impact, one of the most complex mechanical scenarios as strain distributions evolve leading to complex non-symmetric strain distributions. To this end, we take the experimental work recently published by Knutsen et al [49]., where the authors presented *in vivo* mechanical deformations of the brain tissue when subjected to a head impact scenario (neck abrupt rotation). Fig. 5.A shows different maximum principal strain heterogeneous distributions from an axial view of the brain of a volunteer during repeatable mild head rotations. Although ground-breaking, the study mentioned above was limited to low strains to avoid volunteer injury. Thus, the challenge addressed here is to reproduce the complex strain distributions of a local brain region (Fig. 5B) while amplifying the strain magnitudes so actual injury-scenarios could be simulated *in vitro*, i.e., local strains above 21 %. Note that this adds complexity as it requires larger nonlinear deformation patterns [17].

To do so, we identify the relative positions of the magnets that produce such targeted local heterogeneous strains fields. This is done by running a complete set of computational simulations that provides strain measurements in local points of the MRE substrate. These local strains are compared with local measurements from the experimental data to find the solution that better reproduces the *in vivo* scenario. Note that the experimental strains are represented on the undeformed configuration by means of Green-Lagrange strain, to provide a fair comparison with the *in vivo* experimental data. Finally, the obtained magnets positions are experimentally evaluated to validate the approach. These experimental *in vitro* MRE strain patterns are shown in Fig. 5C. All in all, the magneto-mechanical system can reproduce heterogeneous strain distributions close to the real-brain ones, while allowing the amplification of their magnitude by ten times (thus approaching strain thresholds leading to injury).

3.4. From magnetic fields to mechanical forces on cells: application of the stimulation system to evaluate mechanical effects on primary human dermal fibroblasts

To demonstrate the ability of the presented framework to transmit mechanical forces to cellular systems, we designed a set of *in vitro* assays on a well-known study: cellular alignment of human dermal fibroblasts (hFBs) due to mechanical stimulation. These cells are particularly interesting as they play an essential role in the development and repair of tissues [50]. In a recent article, Wahlsten and co-authors conceived a dynamic bioreactor to stimulate skin tissue development [51]. One of the main analyses from this work focuses on the orientation of hFBs responding to mechanical stimulation (cyclic biaxial). These orientation or polarization processes are of high interest in mechanobiology. They have led to insightful discussions on the role of cell alignment in response to mechanical stretch during the last years [52–54]. The published studies rarely alternate different mechanical deforma-

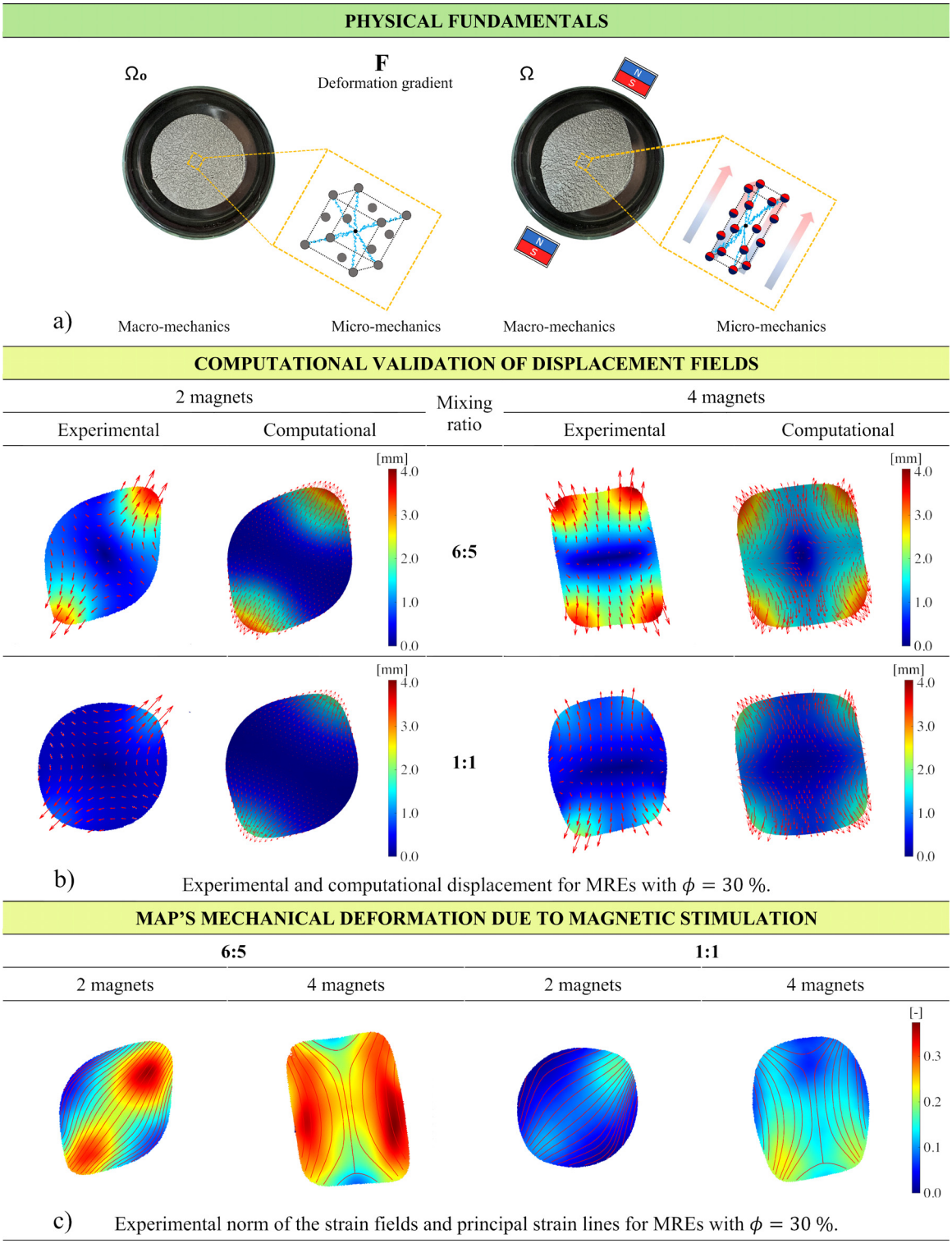

Fig. 4. Multifunctional response and complex strain patterns of MRE samples under magnetic stimulation conditions. (A) Scheme of the micro-mechanical mechanisms and the resultant macro-mechanical deformation of the MRE samples when subjected to an external magnetic field generated by permanent magnets. The particles align along the field direction forming chain-like structures. Then, at a mesoscale level, the formed structures interact with the permanent magnets in the form of macroscopic particle interactions, approaching them. (B) Comparison of experimental data and computational predictions by means of displacement fields, for two different magnetic conditions (i.e., approach of two and four magnets, see Fig. 1) and two different mixing ratios of the MRE's matrix. (C) Experimental results obtained from digital image correlation of local mechanical deformation within MREs with different mixing ratios and two different magnetic conditions (i.e., approach of two and four magnets, see Fig. 1). Note that the position of the permanent magnets corresponds to the closest location to the MRE sample in the experimental setup used along with cellular cultures. These correspond to the maximum magnetic and mechanical deformation fields that can be reached with the present system. All these experiments and computational results correspond to MREs with a particles' volume fraction of 30%.

Table 1
Mechanical response of the MRE substrates under magnetic stimulation and different manufacturing conditions. This table presents MRE samples' macroscopic and microscopic mechanical stiffnesses with different manufacturing parameters: the magnetic particles' volume fraction and elastomeric mixing ratio. These mechanical properties are given for different magnetic conditions and are referred to as: (i) macroscopic stiffness: shear modulus measured from magneto-rheological testing; (ii) microscopic stiffness: Young's modulus obtained from nanoindentation with and without the presence of different sets of permanent magnets. In addition, this table summarizes the local mechanical deformations within the MRE region occupied by cells when using the stimulation device. All the results presented here represent the magneto-mechanical scenarios that occur when using the developed stimulation framework during the cellular assays.

		Multifunctional response of MRE samples				
		Particles' volume	Elastomeric mixing ratio			
	Magnetic conditions	fraction	6:5	1:1	9:10	5:6
Macroscopic stiffness (shear modulus)	0 mT	15 %	0.4	1.5	2.9	3.2
[kPa]		30 %	0.6	2.7	4.6	5.8
	50 mT	15 %	0.7	1.8	3.2	3.4
		30 %	1.0	2.8	5.0	6.2
Microscopic stiffness (Young's modulus)	Independent	Independent 0–30%	4.1	8.4	12.3	
[kPa]	0–50 mT					14.6
Local deformation at MRE center [%]	2 magnets	15 %	14.3	4.0	1.7	1.2
		30 %	21.4	8.5	1.8	1.2
	4 magnets	15 %	16.4	3.4	1.4	1.1
		30 %	24.8	13.3	1.5	1.0

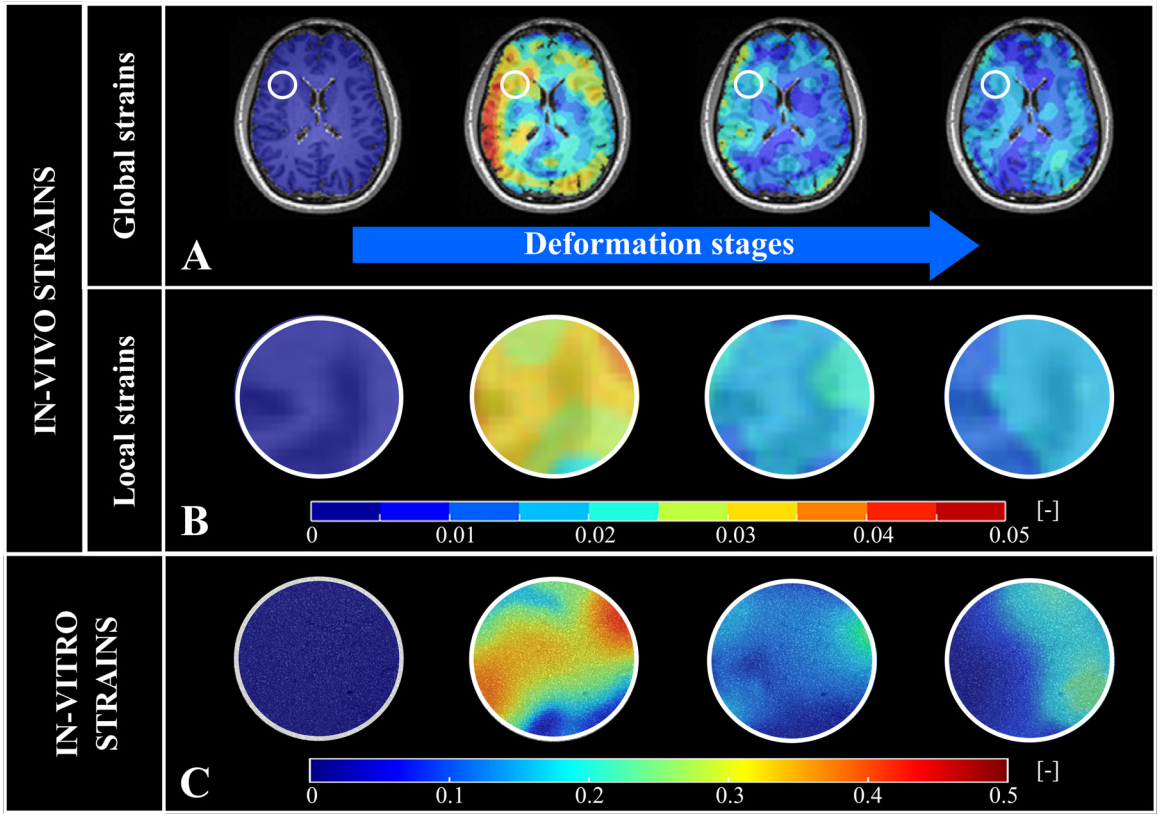

Fig. 5. Proof of concept to evaluate the versatility of the framework to simulate complex heterogeneous strain distributions. (A) *In vivo* strain distribution within an axial view of a human volunteer brain tissue subjected to an abrupt neck rotation, at different impact (deformation) stages. (B) Detail of local strain distributions of the region indicated in (A) with a white circle. The experimental data shown for (A) and (B) are taken from [49]. (C) Experimental strain distribution computed by digital image correlation and plotted on the undeformed configuration of the MRE substrates. Note that the experiments on the MREs (C) aim at reproducing the *in vivo* strain patterns (B) but with an amplification of ten times their magnitude to reach strain values above injury thresholds in traumatic brain injury (≈ 21%).

tion modes within the same assay and are usually limited to either uniaxial or biaxial loading. However, during pathophysiological conditions such as acute injuries, heterogeneous tissue stiffening is associated with changes in the ECM composition [55]. These changes disrupt the mechanical homeostasis that underlies healthy tissue architecture and function, leading to alterations in the cell-generated forces and cellular mechanical properties [56]. Therefore, subsequent changes in the substrate result in heterogeneous strain patterns and temporal-varying interaction forces that affect cellular organization and behavior [57],[58]. In this regard, the resultant cell polarization plays a relevant role in different processes such as collective migration, where a homogeneous orientation of the individuals facilitates mechanical propulsion forces and better intercellular communication [59],[60].

Here, we aim at evaluating the response of primary dermal hFBs, cultured on soft MREs (0.6 kPa shear stiffness), to heterogeneous strain distributions. To this end, hFBs were cultured on the functionalized MRE substrates following the protocol detailed in the Methods section. Then, we subjected the cellular system to different magneto-mechanical conditions. These correspond to the main cases studied, i.e., two and four sets of permanent magnets according to Fig. 4. Although heterogeneous strain patterns

are reached in both cases, the two-magnets scenario approaches a uniaxial loading state and the four-magnets scenario approaches a biaxial loading state. All these tests were analyzed associating cellular polarization with local mechanical conditions and evaluating cell viability (see Methods for details). Local cell analyses were conducted on MRE regions with radial distances from the center below 7.5 mm (see such regions in Fig. 6), thus ensuring negligible strain deviations. Region 1 represents the highest local strain norm (26.0 % and 28.9 % for two magnets and four magnets, respectively), region 2 the center of the MRE sample (21.4 % and 24.8 % for two magnets and four magnets, respectively), and region 3 the lowest local strain norm among them (13.5 % and 20.4 % for two magnets and four magnets, respectively).

The results presented in Fig. 6 indicate a sound transmission of the mechanical forces generated in the substrate to the cells. In the two-magnets stimulation, the effect of local strains is translated into cell alignment towards the principal stretching direction and modulated by the magnitude of these local deformations. Thus, region 1 presents higher cell polarization than region 2, and the latter presents higher polarization than region 3. Moreover, the four-magnets stimulation does not present cell alignment in a clear preferred orientation. All these features are shown by the microscopic images and orientation distributions histograms shown in Figs. 6 and S11. These features suggest that the cellular alignment is determined by two main variables: the deformation state defined as the relation between principal strain components; and the magnitude of such strain components. Thus, a strain state close to uniaxial tension (i.e., one main principal component) promotes cell alignment, and this is modulated by the strain magnitude. However, if the cellular system is exposed to deformation states with no clear principal direction (i.e., close to biaxial loading), the cells do not polarize in a preferred direction.

In addition, we want to highlight that, although no in-depth analyses were conducted herein, we also demonstrated the capability of the system to transmit dynamic loading to the biological material (see cell displacements during magneto-mechanical stimulation in real time, Movie S2 in the supplemental material). Therefore, this proves the validity of the approach to not only reproduce strain patterns on a soft substrate but also to interact with the biological system cultured on it. The present framework thus allows for future work deepening into the effects of heterogeneous mechanical scenarios on the above-mentioned biological processes.

4. Discussion and conclusions

The multi-component imaging-stimulation framework presented opens the possibility of novel *in vitro* fundamental studies to evaluate the effects of mechanics on mechanistic-mediated biological processes. The experimental system, guided by the computational framework, allows for remote modulation of complex strain conditions on the cellular substrate by applying (non-invasive) external magnetic fields. These strain patterns can be controlled in real-time, enabling dynamic modulation of magneto-mechanical loading. In addition, the imaging setup built in this work permits visualizing the cellular process along time on the fly. In the near future, relevant problems within the bioengineering field such as the study of scarring processes [4], wound healing [60,61], cell polarization of immune cells [[53],[62]], proliferation and migration processes in cancer progression [[6,63,64], axonal damage due to mechanical impact [2] or neural crest cell migration [2,21], among others, may take advantage of this system. As an important note, we want to highlight that other research groups can easily adopt the proposed methodology. As a first option, the system can be used within a regular incubator controlling the magnetic fields and, consequently, the mechanical deformation modes over time. Then, the cellular system can be evaluated at different time points in a fluorescence upright microscope. As a second alternative, a multi-compartment MRE can be used manufacturing its central region without magnetic particles. This central transparent region allows for phase contrast imaging on any upright or inverse microscope, making possible to record the cellular dynamics along the whole temporal event (see Movie S3).

With the current solution, large deformation states can be imposed on cellular substrates of around 0.5 to 3 kPa stiffness (in terms of shear modulus). Although this stiffness range is ideal for several biological studies, softer or stiffer substrates may be needed in other scenarios. In this regard, the system allows for using magneto-active hydrogels instead of MRE if softer substrates are required [65]. Indeed, soft enough hydrogels would allow for manufacturing magneto-active substrates with low particles' content allowing for the visualization of cellular systems within a confocal microscope, thus enabling the use of the stimulator system in 3D models. For the use of stiffer substrates, however, the main limitation would be the need for higher magnetic fields to reach significant mechanical deformation. This problem may be solved by opting for larger magnets or using experiment-specific designs optimizing (i.e., reducing) the size of the sample, resulting in much higher magnetic fields for the same magnets.

Contrary to the stimulation used in the specific applications presented in this work, one may study the effect of dynamic substrate stiffness instead of mechanical deformation on cellular processes. The stimulation system developed would also allow this by imposing fixed boundary conditions. In this case, instead of changing its shape, the sample would alternatively undergo internal stress states. Therefore, using a polymeric matrix with a strong nonlinear response (i.e., substantial strain hardening), the application of the external magnetic field will result in a variation of the apparent material stiffness.

Future improvements of the present setup may incorporate a new degree of freedom to allow for azimuthal rotation of the central region holding the substrate and cellular system. This will bring two new possibilities: (1) application of the existing complex deformation modes but changing the initial orientation of the substrate-cellular system; and (2) application of angular displacement while keeping a strong magnetic field with permanent magnets close to the sample, so that material twisting is induced.

Moreover, a current limitation of the stimulation device is the motors' power that limits the stimulation rate. These allow for applied velocities of up to 70 mm/s on the magnets. Although these velocities are high enough to conduct the experiments presented herein and many others (note that stimulation frequencies of 0.1–1 Hz are possible), more complex analysis would require greater velocities to reach high stimulation frequencies. Servomotors substitution can straightforwardly improve this aspect. Further analysis accounting for fast cellular responses would require a deeper consideration of viscous and relaxation mechanisms [[66],[67]]. The frequency-sweeps characterization provided in Figs. S4–S7 allows for estimating the substrate macroscopic stiffness at cyclic stimulation (i.e., storage modulus at the given stimulation frequency). However, although a comprehensive analysis of the viscoelastic and dynamic response of the MRE substrates has been provided, a more detailed experimental analysis using DIC (Fig. 4B) would be needed to evaluate local and macroscopic relaxations within the MRE surface along time. In addition, in its current form, the computational model does not account for such viscous mechanisms and is limited to calculations of the final equilibrium deformation states. This prediction is reliable for the conducted experiments but would be limited for other tests involving variation of stimulation frequencies along time. In addition, some deviations within the peripheral region from perfect symmetric fields were observed in the experimental results. This fact mainly owes to little deviations in the position of the substrate, which may not be per-

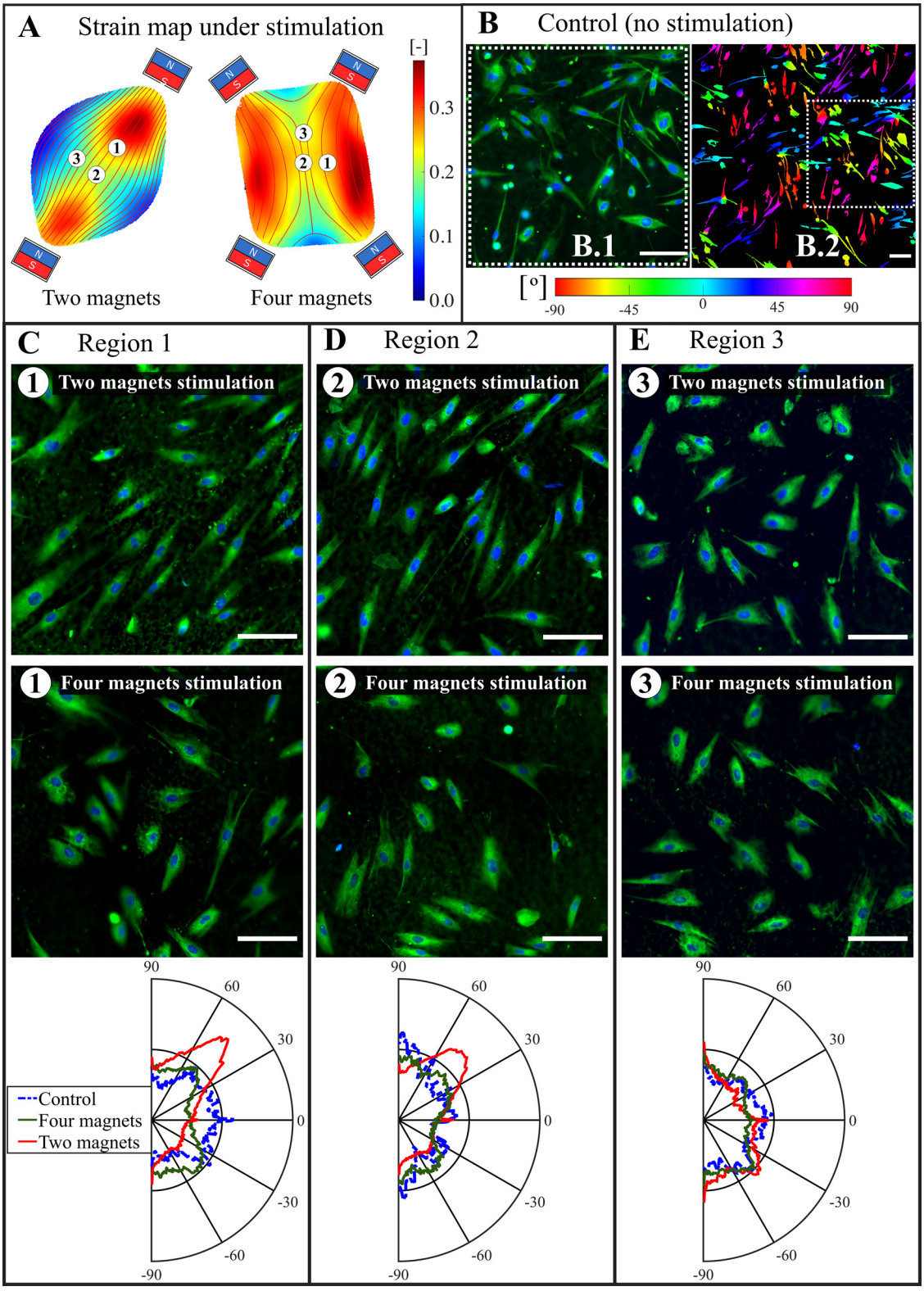

Fig. 6. Proof of concept to evaluate the ability of the framework to transmit forces to the cellular system: cellular polarization dynamics before and after magneto-mechanical stimulation. (A) Distribution of strain magnitude and principal traction forces on the contact surface between the multifunctional substrate and the cell system when subjected to two- and four-opposed permanent magnets presence. (B) Control assay where the cellular system is subjected to null magneto-mechanical stimulation: (B.1) representative cell distribution with nuclei marked in blue and cytoskeleton marked in green; (B.2) orientation distribution of the representative cell distribution in terms of the color map. Note that B.1 presents cellular details within a local region taken from B.2. (C), (D) and (E) show a detail of the cellular arrangement during magneto-mechanical stimulation for the different local regions on the multifunctional substrate indicated in panel A. The upper and mid subpanels present cell distribution with nuclei stained in blue and cytoskeleton in green after two and four magnets stimulation, respectively. The lower subpanel presents the polarization dynamics, where a polar distribution of cell orientation is shown before and after stimulation. These results are for 2 h stimulation. No significant differences between 2 and 24 h stimulations are observed. Note that the magnetic particles present certain autofluorescence that in some figures overlaps with the cellular cytoskeleton stained in green.

fectly centered (note that its sticky nature hinders this endeavor). A potential solution would be adding a bias to the positions of the magnets to compensate such deviations and lead to more symmetric deformations of the substrate. This would require an initial imaging pre-processing of the sample location.

Within mechanical equilibrium, the computational model faithfully describes the magneto-mechanical coupled response but presents some deviations for the stiffer MRE substrates. This behavior is due to the smaller displacement fields reached in such conditions that lead to higher predictive errors. However, it is essential to mention that, in its current form, the model takes as inputs only material parameters with clear physical meaning and that can be controlled during the manufacturing process (note that the same model is applied for different MRE compositions). Adopting phenomenological approaches in the constitutive definition of the energy functions could improve the predictions for a specific MRE substrate (see Eq. (7)). This would be an excellent approach for the use of a very specific MRE substrate. However, we aim at providing a computational framework that not only helps at defining the magnets positions to reach a given deformation for a specific MRE, but also helps at choosing the appropriate MRE composition.

The main outcome of the computational model was to provide physical insights into the magneto-mechanical coupling and, more importantly, guidance during experimental designs to define the relative positions between permanent magnets and the MRE substrate leading to a specific mechanical deformation state (see Fig. S13). Although this has been essential for reproducing complex strain patterns from *in vivo* data (see Fig. 5), we acknowledge that the current approach is computationally expensive for quick designing times (now they take from 5 to 30 min, depending on the specific case). Although this approach can provide good guidance for making on the fly decisions in many biological processes with larger time scales, our view is the use of the computational tool to design the experiment at the beginning. In this regard, the computational tool provides the relative position of the magnets associated to different strain distributions and, then, the user can jump from one to another at any time of the stimulation process. Future work will focus on developing a more extensive set of experimental data providing local strain distributions as a function of permanent magnets' positions. Thus, on top of these data, artificial intelligence algorithms may open the route for *in situ* design of experimental conditions, which can be changed along with the assay on demand. This alternative approach will significantly reduce experimental designing times and facilitate purely automatic determination of the magneto-mechanical conditions. This would also provide better insights into the targeted strain patterns.

Overall, the system designed aims to bring to the next level the creation of customized mechano-stimulation systems for biological matter, suitable thanks to the low magnetic permeability of biological tissues. The anticipated results will offer direct benefits for health purposes by paving the path to models that reproduce mechanistic-mediated biological processes, allowing for unrevealing the underlying mechanisms that take place during physiological scenarios such as traumatic brain injury, pathological skin scarring or fibrotic heart remodeling during myocardial infarction.

CRediT authorship contribution statement

Miguel Angel Moreno-Mateos: Experimental methodology, Computational methodology, Formal analysis, Writing – original draft, Writing – review & editing. **Jorge Gonzalez-Rico:** Experimental methodology, Formal analysis, Writing – review & editing. **Emanuel Nunez-Sardinha:** Prototyping, Writing – review & editing. **Clara Gomez-Cruz:** Visualization, Formal analysis, Writing review & editing. **Maria Luisa Lopez-Donaire:** Formal analysis, Writing – review & editing. **Sergio Lucarini:** Computational methodology, Writing – review & editing. **Angel Arias:** Formal analysis, Writing – review & editing. **Arrate Muñoz-Barrutia:** Visualization, Formal analysis, Writing – review & editing. **Diego Velasco:** Formal analysis, Writing – review & editing. **Daniel Garcia-Gonzalez:** Conceptualization, Prototyping, Experimental methodology, Computational methodology, Formal analysis, Writing – original draft, Writing – review & editing.

Declaration of Competing Interest

The authors declare that they have no known competing financial interests or personal relationships that could have appeared to influence the work reported in this paper.

Acknowledgments

The authors thank Denis Wirtz (Johns Hopkins University) and Jean-Christophe Olivo-Marin (Institute Pasteur) for relevant discussion. The authors acknowledge support from the European Research Council (ERC) under the European Union's Horizon 2020 Research and Innovation Program (Grant agreement No. 947723, project: 4D-BIOMAP), and from Programa de Apoyo a la Realizacion de Proyectos Interdiscisplinares de I+D para Jovenes Investigadores de la Universidad Carlos III de Madrid and Comunidad de Madrid (project: BIOMASKIN). MAMM and CGC acknowledges support from the Ministerio de Ciencia, Innovacion y Universidades, Spain (FPU19/03874 and FPU20/01459) and DGG acknowledges support from the Talent Attraction grant (CM 2018 - 2018-T2/IND-9992) from the Comunidad de Madrid.

Supplementary materials

Supplementary material associated with this article can be found, in the online version, at doi:10.1016/j.apmt.2022.101437.

References

[1] O. Chaudhuri, J. Cooper-White, P.A. Janmey, D.J. Mooney, V.B. Shenoy, Effects of extracellular matrix viscoelasticity on cellular behaviour, Nature 584 (7822) (2020) 535–546, doi:10.1038/s41586-020-2612-2.
[2] M. Tamayo-Elizalde, H. Chen, M. Malboubi, H. Ye, A. Jerusalem, Action potential alterations induced by single F11 neuronal cell loading, Prog. Biophys. Mol. Biol. 162 (2021) 141–153, doi:10.1016/J.PBIOMOLBIO.2020.12.003.
[3] J.M. Grolman, P. Weinand, D.J. Mooney, Extracellular matrix plasticity as a driver of cell spreading, Proc. Natl. Acad. Sci. 117 (42) (2020) 25999–26007, doi:10.1073/PNAS.2008801117.
[4] S. Mascharak, H.E. desJardins-Park, M.F. Davitt, M. Griffin, M.R. Borrelli, A.L. Moore, K. Chen, B. Duoto, M. Chinta, D.S. Foster, A.H. Shen, M. Januszyk, S.H. Kwon, G. Wernig, D.C. Wan, H.P. Lorenz, G.C. Gurtner, M.T. Longaker, Preventing *Engrailed-1* activation in fibroblasts yields wound regeneration without scarring, Science 372 (6540) (2021), doi:10.1126/SCIENCE.ABA2374.
[5] A. Alert, X. Trepat, Physical models of collective cell migration, Annu. Rev. Condens. Matter Phys. 11 (2020) 77–101, doi:10.1146/annurev-conmatphys-031218-013516.
[6] E.O. Wisniewski, P. Mistriotis, K. Bera, R.A. Law, J. Zhang, M. Nikolic, M. Weiger, M. Parlani, S. Tuntithavornwat, A. Afthinos, R. Zhao, D. Wirtz, P. Kalab, G. Scarcelli, P. Friedl, K. Konstantopoulos, Dorsoventral polarity directs cell responses to migration track geometries, Sci. Adv. 6 (31) (2020) 6505–6536, doi:10.1126/SCIADV.ABA6505.
[7] F. Bianchi, J.H. George, M. Malboubi, A. Jerusalem, M.S. Thompson, H. Ye, Engineering a uniaxial substrate-stretching device for simultaneous electrophysiological measurements and imaging of strained peripheral neurons, Med. Eng. Phys. 67 (2019) 1–10, doi:10.1016/J.MEDENGPHY.2019.02.014.
[8] J. Hu, Y. Li, Y. Hao, T. Zheng, S.K. Gupta, G.A. Parada, H. Wu, S. Lin, S. Wang, X. Zhao, R.D. Goldman, S. Cai, M. Guo, High stretchability, strength, and toughness of living cells enabled by hyperelastic vimentin intermediate filaments, Proc. Natl. Acad. Sci. 116 (35) (2019) 17175–17180, doi:10.1073/PNAS.1903890116.
[9] L. Chen, C. Yan, Z. Zheng, Functional polymer surfaces for controlling cell behaviors, Mater. Today 21 (1) (2018) 38–59, doi:10.1016/J.MATTOD.2017.07.002.
[10] X. Wang, Q. Gao, X. Han, B. Bu, L. Wang, A. Li, L. Deng, Sensitive detection of cell-derived force and collagen matrix tension in microtissues undergoing large-scale densification, Proc. Natl. Acad. Sci. 118 (36) (2021), doi:10.1073/PNAS.2106061118.

[11] M. Walker, P. Rizzuto, M. Godin, AE. Pelling, Structural and mechanical remodeling of the cytoskeleton maintains tensional homeostasis in 3D microtissues under acute dynamic stretch, Sci. Rep. 10 (1) (2020) 1–16 *2020 10:1*, doi:10.1038/s41598-020-64725-7.
[12] C. Fang, X. Wei, X. Shao, Y. Lin, Force-mediated cellular anisotropy and plasticity dictate the elongation dynamics of embryos, Sci. Adv. 7 (27) (2021), doi:10.1126/SCIADV.ABG3264.
[13] D. Park, E. Wershof, S. Boeing, A. Labernadie, R.P. Jenkins, S. George, X. Trepat, P.A. Bates, E. Sahai, Extracellular matrix anisotropy is determined by TFAP2C-dependent regulation of cell collisions, Nat. Mater. 19 (2) (2019) 227–238 *2019 19:2*, doi:10.1038/s41563-019-0504-3.
[14] F. Wei, X. Xu, C. Zhang, Y. Liao, B. Ji, N. Wang, Stress fiber anisotropy contributes to force-mode dependent chromatin stretching and gene upregulation in living cells, Nat. Commun. 11 (1) (2020) 1–12 *2020 11:1*, doi:10.1038/s41467-020-18584-5.
[15] S. Goren, Y. Koren, X. Xu, A. Lesman, Elastic Anisotropy governs the range of cell-induced displacements, Biophys. J. 118 (5) (2020) 1152–1164, doi:10.1016/J.BPJ.2019.12.033.
[16] C.A. Tagge, A.M. Fisher, O.V. Minaeva, A. Gaudreau-Balderrama, J.A. Moncaster, X.L. Zhang, M.W. Wojnarowicz, N. Casey, H. Lu, O.N. Kokiko-Cochran, S. Saman, M. Ericsson, K.D. Onos, R. Veksler, V.V. Senatorov, A. Kondo, X.Z. Zhou, O. Miry, L.R. Vose, et al., Concussion, microvascular injury, and early tauopathy in young athletes after impact head injury and an impact concussion mouse model, Brain 141 (2) (2018) 422–458, doi:10.1093/brain/awx350.
[17] D. Garcia-Gonzalez, N.S. Race, N.L. Voets, D.R. Jenkins, S.N. Sotiropoulos, G. Acosta, M. Cruz-Haces, J. Tang, R. Shi, A. Jérusalem, Cognition based bTBI mechanistic criteria; a tool for preventive and therapeutic innovations, Sci. Rep. 8 (1) (2018) 10273, doi:10.1038/s41598-018-28271-7.
[18] K. Pogoda, PA. Janmey, Glial tissue mechanics and mechanosensing by glial cells, Front. Cell. Neurosci. 12 (2018) 25, doi:10.3389/FNCEL.2018.00025.
[19] M. Gómez-González, E. Latorre, M. Arroyo, X. Trepat, Measuring mechanical stress in living tissues, Nat. Rev. Phys. 2 (6) (2020) 300–317 *2020 2:6*, doi:10.1038/s42254-020-0184-6.
[20] N.R. Chevalier, E. Gazquez, L. Bidault, T. Guilbert, C. Vias, E. Vian, Y. Watanabe, L. Muller, S. Germain, N. Bondurand, S. Dufour, V. Fleury, How tissue mechanical properties affect enteric neural crest cell migration, Sci. Rep. 6 (1) (2016) 1–18 *2016 6:1*, doi:10.1038/srep20927.
[21] E.H. Barriga, K. Franze, G. Charras, R. Mayor, Tissue stiffening coordinates morphogenesis by triggering collective cell migration *in vivo*, Nature 554 (7693) (2018) 523–527 *2018 554:7693*, doi:10.1038/nature25742.
[22] A. Shellard, R. Mayor, Integrating chemical and mechanical signals in neural crest cell migration, Curr. Opin. Genet. Dev. 57 (2019) 16–24, doi:10.1016/J.GDE.2019.06.004.
[23] Y. Zheng, M.K.L. Han, Q. Jiang, B. Li, J. Feng, Campo A del. 4D hydrogel for dynamic cell culture with orthogonal, wavelength-dependent mechanical and biochemical cues, Mater. Horiz. 7 (1) (2020) 111–116, doi:10.1039/C9MH00665F.
[24] M. Mayer, R. Rabindranath, J. Börner, E. Hörner, A. Bentz, J. Salgado, H. Han, H. Böse, J. Probst, M. Shamonin, G.J. Monkman, G. Schlunck, Ultra-soft PDMS-based magnetoactive elastomers as dynamic cell culture substrata, PLoS One 8 (10) (2013), doi:10.1371/journal.pone.0076196.
[25] E.A. Corbin, A. Vite, E.G. Peyster, M. Bhoopalam, J. Brandimarto, X. Wang, A.I. Bennett, A.T. Clark, X. Cheng, K.T. Turner, K. Musunuru, K.B. Margulies, Tunable and reversible substrate stiffness reveals a dynamic mechanosensitivity of cardiomyocytes, ACS Appl. Mater. Interfaces 11 (23) (2019) 20603–20614, doi:10.1021/ACSAMI.9B02446.
[26] F.E. Uslu, C.D. Davidson, E. Mailand, N. Bouklas, B.M. Baker, M.S. Sakar, Engineered extracellular matrices with integrated wireless microactuators to study mechanobiology, Adv. Mater. 33 (40) (2021) 2102641, doi:10.1002/ADMA.202102641.
[27] Z. Ren, R. Zhang, R.H. Soon, Z. Liu, W. Hu, P.R. Onck, M. Sitti, Soft-bodied adaptive multimodal locomotion strategies in fluid-filled confined spaces, Sci. Adv. 7 (27) (2021), doi:10.1126/SCIADV.ABH2022.
[28] D. Son, M.C. Ugurlu, M. Sitti, Permanent magnet array–driven navigation of wireless millirobots inside soft tissues, Sci. Adv. 7 (43) (2021), doi:10.1126/SCIADV.ABI8932.
[29] J. Zhang, Y. Guo, W. Hu, M. Sitti, Wirelessly actuated thermo- and magneto-responsive soft bimorph materials with programmable shape-morphing, Adv. Mater. 33 (30) (2021) 2100336, doi:10.1002/adma.202100336.
[30] A.K. Bastola, M. Hossain, A review on magneto-mechanical characterizations of magnetorheological elastomers, Compos. Part B Eng. 200 (2020) 108348, doi:10.1016/j.compositesb.2020.108348.
[31] J. Blaber, B. Adair, A. Antoniou, Ncorr: open-source 2D digital image correlation matlab software, Exp. Mech. 55 (6) (2015) 1105–1122 *2015 55:6*, doi:10.1007/S11340-015-0009-1.
[32] D. Garcia-Gonzalez, C.M. Landis, Magneto-diffusion-viscohyperelasticity for magneto-active hydrogels: Rate dependences across time scales, J. Mech. Phys. Solids 139 (2020) 103934, doi:10.1016/J.JMPS.2020.103934.
[33] C. Dorn, L. Bodelot, K. Danas, Experiments and numerical implementation of a boundary value problem involving a magnetorheological elastomer layer subjected to a nonuniform magnetic field, J. Appl. Mech. 88 (7) (2021), doi:10.1115/1.4050534.
[34] P. Saxena, J.P. Pelteret, P. Steinmann, Modelling of iron-filled magneto-active polymers with a dispersed chain-like microstructure, Eur. J. Mech. A Solids 50 (2015) 132–151, doi:10.1016/J.EUROMECHSOL.2014.10.005.
[35] E. Salas, R. Bustamante, Numerical solution of some boundary value problems in nonlinear magneto-elasticity, J. Intell. Mater. Syst. Struct. 26 (2) (2015) 156–171, doi:10.1177/1045389X14522533.
[36] D. Mukherjee, M. Rambausek, K. Danas, An explicit dissipative model for isotropic hard magnetorheological elastomers, J. Mech. Phys. Solids 151 (2021) 104361, doi:10.1016/J.JMPS.2021.104361.
[37] E. Psarra, L. Bodelot, K. Danas, Wrinkling to crinkling transitions and curvature localization in a magnetoelastic film bonded to a non-magnetic substrate, J. Mech. Phys. Solids 133 (2019) 103734, doi:10.1016/J.JMPS.2019.103734.
[38] E. Psarra, L. Bodelot, K. Danas, Two-field surface pattern control *via* marginally stable magnetorheological elastomers, Soft Matter 13 (37) (2017) 6576–6584, doi:10.1039/C7SM00996H.
[39] C. Dorn, L. Bodelot, K. Danas, Experiments and numerical implementation of a boundary value problem involving a magnetorheological elastomer layer subjected to a nonuniform magnetic field, J. Appl. Mech. 88 (7) (2021), doi:10.1115/1.4050534.
[40] Z. Püspöki, M. Storath, D. Sage, M. Unser, Transforms and operators for directional bioimage analysis: a survey, Adv. Anat. Embryol. Cell Biol. 219 (2016) 69–93, doi:10.1007/978-3-319-28549-8_3.
[41] M. Rambausek, D. Mukherjee, K. Danas, A computational framework for magnetically hard and soft viscoelastic magnetorheological elastomers, Comput. Methods Appl. Mech. Eng. 391 (2022) 114500, doi:10.1016/j.cma.2021.114500.
[42] M.A. Moreno, J. Gonzalez-Rico, M.L. Lopez-Donaire, A. Arias, D. Garcia-Gonzalez, New experimental insights into magneto-mechanical rate dependences of magnetorheological elastomers, Compos. Part B Eng. 224 (2021) 109148, doi:10.1016/J.COMPOSITESB.2021.109148.
[43] D. Garcia-Gonzalez, M.A. Moreno, L. Valencia, A. Arias, D. Velasco, Influence of elastomeric matrix and particle volume fraction on the mechanical response of magneto-active polymers, Compos. Part B Eng. 215 (2021) 108796, doi:10.1016/J.COMPOSITESB.2021.108796.
[44] T.J. Lampert, N. Kamprad, M. Edwards, J. Borleis, A.J. Watson, M. Tarantola, P.N. Devreotes, Shear force-based genetic screen reveals negative regulators of cell adhesion and protrusive activity, Proc. Natl. Acad. Sci. 114 (37) (2017) E7727–E7736, doi:10.1073/PNAS.1616600114.
[45] A.M. Reyes Lua, R. Hopf, E. Mazza, Factors influencing the mechanical properties of soft elastomer substrates for traction force microscopy, Mech. Soft Mater. 2 (1) (2020) 1–12 *2020 2:1*, doi:10.1007/S42558-020-00021-8.
[46] D. Garcia-Gonzalez, M. Hossain, A microstructural-based approach to model magneto-viscoelastic materials at finite strains, Int. J. Solids Struct. (2021) 208–209 119-132, doi:10.1016/J.IJSOLSTR.2020.10.028.
[47] H. Wu, Z. Xu, J. Wang, X. Bo, Z. Tang, S. Jiang, G. Zhang, Chain formation mechanism of magnetic particles in magnetorheological elastomers during prestructure, J. Magn. Magn. Mater. 527 (2021) 167693, doi:10.1016/J.JMMM.2020.167693.
[48] S. Mascharak, H.E. desJardins-Park, M.F. Davitt, M. Griffin, M.R. Borrelli, A.L. Moore, K. Chen, B. Duoto, M. Chinta, D.S. Foster, A.H. Shen, M. Januszyk, S.H. Kwon, G. Wernig, D.C. Wan, H.P. Lorenz, G.C. Gurtner, M.T. Longaker, Preventing Engrailed-1 activation in fibroblasts yields wound regeneration without scarring, Science 372 (6540) (2021), doi:10.1126/SCIENCE.ABA2374.
[49] A.K. Knutsen, A.D. Gomez, M. Gangolli, W.T. Wang, D. Chan, Y.C. Lu, E. Christoforou, J.L. Prince, P.v. Bayly, J.A. Butman, D.L. Pham, *In vivo* estimates of axonal stretch and 3D brain deformation during mild head impact, Brain Multiphys. 1 (2020) 100015, doi:10.1016/J.BRAIN.2020.100015.
[50] B. Hinz, S.H. Phan, V.J. Thannickal, A. Galli, M.L. Bochaton-Piallat, G. Gabbiani, The myofibroblast: one function, multiple origins, Am. J. Pathol. 170 (6) (2007) 1807–1816, doi:10.2353/AJPATH.2007.070112.
[51] A. Wahlsten, D. Rütsche, M. Nanni, C. Giampietro, T. Biedermann, E. Reichmann, E. Mazza, Mechanical stimulation induces rapid fibroblast proliferation and accelerates the early maturation of human skin substitutes, Biomaterials 273 (February) (2021) 120779, doi:10.1016/j.biomaterials.2021.120779.
[52] K. Chen, A. Vigliotti, M. Bacca, R.M. McMeeking, V.S. Deshpande, J.W. Holmes, Role of boundary conditions in determining cell alignment in response to stretch, Proc. Natl. Acad. Sci. 115 (5) (2018) 986–991, doi:10.1073/PNAS.1715059115.
[53] H. Atcha, A. Jairaman, J.R. Holt, V.S. Meli, R.R. Nagalla, P.K. Veerasubramanian, K.T. Brumm, H.E. Lim, S. Othy, M.D. Cahalan, M.M. Pathak, W.F. Liu, Mechanically activated ion channel Piezo1 modulates macrophage polarization and stiffness sensing, Nat. Commun. 12 (1) (2021) 1–14 *2021 12:1*, doi:10.1038/s41467-021-23482-5.
[54] R. Emig, C.M. Zgierski-Johnston, V. Timmermann, A.J. Taberner, M.P. Nash, P. Kohl, R. Peyronnet, Passive myocardial mechanical properties: meaning, measurement, models, Biophys. Rev. 13 (5) (2021) 587–610 *2021 13:5*, doi:10.1007/S12551-021-00838-1.
[55] P.C. Georges, J.J. Hui, Z. Gombos, M.E. McCormick, A.Y. Wang, M. Uemura, R. Mick, P.A. Janmey, E.E. Furth, R.G. Wells, Increased stiffness of the rat liver precedes matrix deposition: implications for fibrosis, Am. J. Physiol. - Gastrointest. Liver Physiol. 293 (6) (2007) 1147–1154, doi:10.1152/AJPGI.00032.2007.
[56] J.D. Humphrey, E.R. Dufresne, MA. Schwartz, Mechanotransduction and extracellular matrix homeostasis, Nat. Rev. Mol. Cell Biol. 15 (12) (2014) 802–812 *2014 15:12*, doi:10.1038/nrm3896.
[57] E. Kingham, R.O.C. Oreffo, Embryonic and induced pluripotent stem cells: understanding, creating, and exploiting the nano-niche for regenerative medicine, ACS Nano 7 (3) (2013) 1867–1881, doi:10.1021/NN3037094.
[58] N.A. Kurniawan, P.K. Chaudhuri, C.T. Lim, Mechanobiology of cell migration in the context of dynamic two-way cell–matrix interactions, J. Biomech. 49 (8) (2016) 1355–1368, doi:10.1016/J.JBIOMECH.2015.12.023.

[59] D. Garcia-Gonzalez, A. Muñoz-Barrutia, Computational insights into the influence of substrate stiffness on collective cell migration, Extrem. Mech. Lett. 40 (2020) 100928, doi:10.1016/J.EML.2020.100928.
[60] R. Sunyer, V. Conte, J. Escribano, A. Elosegui-Artola, A. Labernadie, L. Valon, D. Navajas, J.M. García-Aznar, J.J. Muñoz, P. Roca-Cusachs, X. Trepat, Collective cell durotaxis emerges from long-range intercellular force transmission, Science 353 (6304) (2016) 1157–1161, doi:10.1126/SCIENCE.AAF7119.
[61] C. Valero, E. Javierre, J.M. García-Aznar, M.J. Gómez-Benito, A. Menzel, Modeling of anisotropic wound healing, J. Mech. Phys. Solids 79 (2015) 80–91, doi:10.1016/J.JMPS.2015.03.009.
[62] V.S. Meli, H. Atcha, P.K. Veerasubramanian, R.R. Nagalla, T.U. Luu, E.Y. Chen, C.F. Guerrero-Juarez, K. Yamaga, W. Pandori, J.Y. Hsieh, T.L. Downing, D.A. Fruman, M.B. Lodoen, M.V. Plikus, W. Wang, W.F. Liu, YAP-mediated mechanotransduction tunes the macrophage inflammatory response, Sci. Adv. 6 (49) (2020), doi:10.1126/SCIADV.ABB8471.
[63] J. Dai, Y. Wang, J. Gong, Y. Yao, Biointerface anisotropy modulates migration of breast cancer cell, Colloids Surf. B 190 (2020) 110973, doi:10.1016/J.COLSURFB.2020.110973.
[64] P.H. Wu, D.M. Gilkes, J.M. Phillip, A. Narkar, T.W.T. Cheng, J. Marchand, M.H. Lee, R. Li, D. Wirtz, Single-cell morphology encodes metastatic potential, Sci. Adv. 6 (4) (2020), doi:10.1126/SCIADV.AAW6938.
[65] X. Liu, Y. Yang, M.E. Inda, S. Lin, J. Wu, Y. Kim, X. Chen, D. Ma, T.K. Lu, X. Zhao, Magnetic living hydrogels for intestinal localization, retention, and diagnosis, Adv. Funct. Mater. 31 (27) (2021) 2010918, doi:10.1002/ADFM.202010918.
[66] I. Andreu, B. Falcones, S. Hurst, N. Chahare, X. Quiroga, A.L. le Roux, Z. Kechagia, A.E.M. Beedle, A. Elosegui-Artola, X. Trepat, R. Farré, T. Betz, I. Almendros, P. Roca-Cusachs, The force loading rate drives cell mechanosensing through both reinforcement and cytoskeletal softening, Nat. Commun. 12 (1) (2021) 1–12 *2021 12:1*, doi:10.1038/s41467-021-24383-3.
[67] K. Adebowale, Z. Gong, J.C. Hou, K.M. Wisdom, D. Garbett, N.S. Lee Hpyo, T. Meyer, D.J. Odde, V.B. Shenoy, O. Chaudhuri, Enhanced substrate stress relaxation promotes filopodia-mediated cell migration, Nat. Mater. 20 (9) (2021) 1290–1299 *2021 20:9*, doi:10.1038/s41563-021-00981-w.